Journal of Catalysis 276 (2010) 280–291

Contents lists available at ScienceDirect

Journal of Catalysis

journal homepage: www.elsevier.com/locate/jcat

Water–gas shift catalysts based on ionic liquid mediated supported Cu nanoparticles

Richard Knapp, Sonja A. Wyrzgol, Andreas Jentys *, Johannes A. Lercher

Lehrstuhl II für Technische Chemie, Technische Universität München, Lichtenbergstr. 4, D-85747 Garching, Germany

ARTICLE INFO

Article history:
Received 3 May 2010
Revised 17 September 2010
Accepted 19 September 2010
Available online 25 October 2010

Keywords:
Ionic liquids
Supported catalysts
Copper nanoparticles
EXAFS
XANES
In situ IR spectroscopy
Low-temperature water–gas shift

ABSTRACT

The sorptive and catalytic properties of alumina supported Cu nanoparticles coated with a thin film of 1-butyl-2,3-dimethyl-imidazolium trifluoromethane sulfonate (BDiMIm) for low-temperature water–gas shift have been explored. For uncoated catalysts, the rate per gram catalyst passed through a maximum with increasing concentration of oxygen on the Cu surface. For reduced catalysts, the presence of oxygen facilitates the dissociation of water, while in excess it decreases the reaction rates due to limiting the reactant concentration. Catalysts coated with ionic liquid showed a higher turn over frequency for the water–gas shift reaction at low temperatures compared to uncoated catalysts and to the best commercial systems, which is attributed to a higher concentration of water in the proximity of the active sites and to the facile decomposition of carboxyl intermediates by the interaction with the ionic liquid. In addition, the presence of the ionic liquid reduces the sorption strength of CO leading to a better balance of the reactants at the surface.

1. Introduction

The water–gas shift reaction (Eq. (1)) allows adjusting the CO to H_2 ratio in synthesis gas. Since the reaction is exothermic, the formation of hydrogen is favored at low temperatures and, therefore, the lower limit for the CO concentration achievable decreases with decreasing temperature. For example, the exit stream after the water–gas shift reaction at approximately 200 °C contains less than 0.5% CO [1].

$$CO + H_2O \rightleftharpoons CO_2 + H_2 \quad \Delta H^o = -41\ kJ/mol \tag{1}$$

In industrial implementations, the water–gas shift reaction is performed in two steps, a high-temperature and a low-temperature reaction. The low-temperature water–gas shift reaction (LTWGS) is performed at temperatures between 210 and 250 °C over catalysts based on copper supported on zinc oxide. These catalysts are pyrophoric and deactivate in the presence of liquid water and by thermal sintering. Moreover, a clean feed is needed in order to avoid deactivation by sulfur and halides. Since the reaction is reversible, the rate of the CO conversion is reduced by the presence of the products CO_2 and H_2 [2].

Two different reaction mechanisms, the associative and the surface redox mechanisms have been discussed for LTWGS [3–10]. Recent publications show that in the reaction pathway of the associative mechanism $^*CO$ reacts with $^*OH$ groups to a formyl (carboxyl) species ($^*COOH$) [5,11]. Under these conditions, formate species can also be formed by CO_2 hydrogenation acting as stable spectator species. The elementary steps are compiled in Eqs. (2)–(6) [5]. Water and CO adsorb on the catalyst surface, and the dissociation of the adsorbed water is reported to be the reaction with the first significant energy barrier. Its height depends on the Cu particle size and varies between 86 and 135 kJ mol^{-1} being about seven times higher than the barrier to desorb molecular H_2O [4,5]. Thus, from the energetic point of view, the abstraction of hydrogen from water seems to be the rate-controlling step [5]. The nature of the transition state and the energy barrier depend on the catalyst and its surface properties. Adsorbed CO and OH react to $^*COOH$ and the carboxyl species decompose to the products H_2 and CO_2 desorbing in the last step from the catalyst surface. The decomposition of $^*COOH$ is the second step with a high energy barrier. The calculated potential energy diagram and the formed intermediate species are depicted in Fig. S1.

$$H_2O_{(g)} + * \rightleftharpoons H_2O^* \tag{2}$$

$$H_2O^* + * \rightleftharpoons {}^*OH + H^* \tag{3}$$

$$CO_{(g)} + * \rightleftharpoons {}^*CO \tag{4}$$

$$^*OH + {}^*CO \rightleftharpoons {}^*COOH + * \tag{5}$$

$$2\,{}^*COOH \rightleftharpoons CO_{2(g)} + H_2 + 2^* \tag{6}$$

The second reaction mechanism described in the literature is the surface redox mechanism [7]. The first step is the adsorption of water on the catalyst surface and its dissociation to oxygen and

* Corresponding author. Fax: +49 8928913544.
E-mail address: andreas.jentys@ch.tum.de (A. Jentys).

0021-9517/$ - see front matter © 2010 Elsevier Inc. All rights reserved.
doi:10.1016/j.jcat.2010.09.019

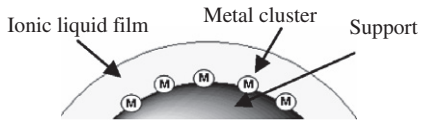

Fig. 1. Catalyst concept with metal clusters (1–2 nm) immobilized in thin films of ionic liquid (2–5 nm).

hydrogen, followed by a bond formation between oxygen and absorbed CO. The rate-determining step depends on the partial pressure of the reactants [8]. Hydrogen and CO_2 adsorbed on Cu(1 0 0) surfaces can form formate species, which block the active sites of the catalyst. These formate species can undergo hydrogenation to methanol, but since their surface concentration is low under industrial conditions, the formation of methanol is not very important [9].

It is generally assumed that both reaction pathways may occur under low-temperature water–gas shift conditions over copper-based catalysts and as the reaction is reported to be structure sensitive, the particle size should play a major role in the associative mechanism [10].

Modifying the local concentration of reactants and products at the active sites, e.g., by using an environment with different solubilities of the gases, appears to be an option to enhance the activity of the catalysts. In the particular case, we intended to improve the availability of water in the water–gas shift reaction by the presence of the ionic liquid. Supported ionic liquid catalysts [12–15] are a special variant of supported liquid phase catalysts [16] in which the catalytically active components are immobilized in the ionic liquid. Due to the low vapor pressure of the ionic liquid, these catalysts can be readily applied in gas phase reactions [17]. The interactions of the ionic liquid with the support as well as with the active component have been studied showing ordering phenomena and domain formation of the ionic liquid [15,18,19]. Catalysts with immobilized ionic liquids were successfully used in reactions such as hydroformylation of olefins [12], achiral hydrogenation [20], the Heck reaction [21], hydroamination [13,14] and hydrogenation [15]. A schematic drawing of a supported ionic liquid catalyst with metal nanoparticles as the active component immobilized on an alumina support is depicted in Fig. 1.

The current contribution focuses on the synthesis and characterization of catalysts based on ionic liquid (1-butyl-2,3-dimethyl-imidazolium trifluoromethane sulfonate) mediated Cu nanoparticles as catalysts for the low-temperature water–gas shift reaction. The correlation between the oxidation state of the metal and the reactivity in the low-temperature water–gas shift reaction as well as the enhanced turn over frequencies of the coated system at lower temperatures is addressed using *in situ* XAFS and IR spectroscopy in combination with investigating the activity for the low-temperature WGS reaction. Furthermore, the influence of the specific surface area of the support on the copper particle size and the reduction degree are discussed.

2. Experimental

2.1. Materials

The ionic liquid 1-butyl-2,3-dimethyl-imidazolium trifluoromethane sulfonate (BDiMIm) (99%) with a maximum water and halide content of 48 and 103 ppm, respectively, was provided by Solvent Innovation GmbH. Copper(II) nitrate trihydrate (99%) and methanol (99.8%) were obtained from Aldrich. The γ-alumina supports with pore volumes between 0.3 and 0.98 mL g^{-1} and the Shift-Max-240 catalyst were provided by Süd Chemie AG. All chemicals were used as received. CO (purity 4.0), CO_2 (purity 4.5), Ar (purity 5.0), H_2 (purity 5.0) and N_2 (purity 5.0) were purchased from Westfalen.

2.2. Preparation of the supported catalysts

Before use, the series of alumina supports was dried at 200 °C for two hours. Cu was loaded onto the supports (5 wt.% metal) by incipient wetness impregnation using an aqueous solution of copper(II) nitrate trihydrate. After impregnation, water was removed by freeze drying. The materials were calcined at 300 °C for 3 h and at 450 °C for 4 h in synthetic air and subsequently reduced at 215 °C for 3 h in hydrogen flow.

For preparing supported ionic liquid catalysts, the corresponding Cu/Al_2O_3 catalysts were added to a solution of BDiMIm dissolved in methanol. The suspension was stirred at room temperature for 10 min, and the volatile components were slowly removed by freeze drying to give a free flowing black powder ($Cu/BDiMIm/Al_2O_3$).

The BET surface areas, pore volumes and pore radii of the γ-Al_2O_3 supports are listed in Table 1.

2.3. Characterization

The copper content of the supported catalysts was determined by atomic absorption spectroscopy using a UNICAM 939 spectrometer. The concentration of ionic liquid adsorbed on the surface was determined by elemental analysis.

IR spectra were measured on a Bruker IFS 88 spectrometer using a vacuum and a flow cell in transmission mode. The spectra were recorded at a resolution of 4 cm^{-1} in the region from 4000 to 400 cm^{-1}. The samples were pressed into self-supporting wafers (of ca. 5 mg) and activated in vacuum for 1 h at 120 °C or in He flow at 120 °C for 1 h. The reduction was carried out at 215 °C and 0.8 bar hydrogen for 60 min for the vacuum experiments and in a hydrogen/helium mixture at 215 °C for 60 min for the experiments under flow conditions. CO, CO_2 and D_2O were dosed at pressures of 0.01, 0.05, 0.1, 0.5, 1.0 and 1.5 mbar (note that for CO adsorbed on the coated catalyst only adsorption at the four latter pressures is reported) and room temperature. For the reaction, a gas mixture of 2.5 mL min^{-1} CO and 2.5 mL min^{-1} H_2O diluted in 20 mL min^{-1} He was used.

The X-ray absorption spectra were collected at the beamline X1 at HASYLAB, DESY, Hamburg, Germany and at the beamline BM26A at the ESRF, Grenoble, France. The Si(1 1 1) double-crystal monochromator was detuned to 60% of the maximum intensity to minimize the intensity of the higher harmonics in the X-ray beam. The catalysts were pressed into self-supporting wafers (ca. 150 mg), and the X-ray absorption spectra were collected at the Cu K edge (8979 eV) in He flow at liquid N_2 temperature for EXAFS analysis and at room temperature or under *in situ* conditions during activation to 250 °C in a H_2/He mixture and reaction (150 °C with a CO, He and water flow with the same composition as used for the *in situ* IR experiments). Please note that prior to the *in situ* activity tests, the samples were activated at 215 °C. The XAFS data were analyzed using the *Six Pack* software [22]. For EXAFS analysis, the scattering contributions of the background were removed from

Table 1
BET surface areas, pore volumes and pore radii of used support materials.

Support	BET surface area ($m^2 g^{-1}$)	Pore volume (mL g^{-1})	Pore radius (nm)
Al_2O_3-54	54	0.30	21.9
Al_2O_3-99	99	0.51	12.0
Al_2O_3-100	100	0.55	20.7
Al_2O_3-149	149	0.52	13.4
Al_2O_3-151	151	0.74	19.5
Al_2O_3-214	214	0.52	9.7
Al_2O_3-257	257	0.98	7/500 (bimodal)
Al_2O_3-360	360	0.30	3.5

the X-ray absorption by a third-order polynomial function. The oscillations were weighted with k^2 and Fourier-transformed within the limit $k = 3.5–12$ Å^{-1}. The local environment of the Cu atoms was determined from the EXAFS using the phase shift and amplitude function for Cu–Cu and Cu–O calculated including multiple scattering processes (FEFF version 8.40) [23,24].

For the analysis of the XANES, the spectra were normalized to unity using the *XANES dactyloscope* software [25]. The position of the edge was calibrated using the spectra of a Cu reference-foil measured simultaneously.

To further confirm the accessible copper surface area obtained by the XAFS measurements, N_2O chemisorption experiments were performed using the reactive frontal chromatography method [26]. For each experiment, 500 mg catalyst (activated *in situ* at 250 °C for 60 min) was used.

2.4. Catalytic activity

The low-temperature water–gas shift reaction was studied at temperatures between 160 and 250 °C and a pressure of 2 bar. The gas composition used was $p(H_2) = 0.53$ (75%), $p(CO) = 0.05$ (8%), $p(CO_2) = 0.08$ (13%) and $p(N_2) = 0.03$ (4%), at a steam to gas ratio of 3–7 (total gas flow 40 mL min^{-1}). A fixed bed reactor filled with 200 mg catalyst (diluted with SiC) was used. The products were analyzed using a Shimadzu GC-2014 gas chromatograph. For comparison, also a commercial catalyst (ShiftMax-240) was also tested at temperatures between 160 and 250 °C. The activity of the catalysts is either presented as turn over frequency or presented as rate per gram catalyst to evaluate the performance of the catalysts (all catalysts had the same copper loading). The equations used for the kinetic analysis at differential and integral reaction conditions are presented in Supplementary material.

3. Results

3.1. Activity of the uncoated catalysts

The turn over frequencies of the uncoated Cu/Al_2O_3 catalysts in the low-temperature water–gas shift reaction as function of temperature are shown in Fig. 2, the apparent energies of activation are given in Table 2.

The turn over frequencies for the water–gas shift reaction were determined at feed compositions close to industrial conditions (H_2 to CO ratio of ca. 9 and a CO_2 to CO ratio of 1.6). The TOF for a CuO/Al_2O_3 catalyst of 0.8×10^{-6} mol m^{-2} s^{-1} at 200 °C reported [27] is higher than the TOF observed for the Cu/Al_2O_3-149 catalyst at 200 °C (0.3×10^{-6} mol m^{-2} s^{-1}), which resulted from the different

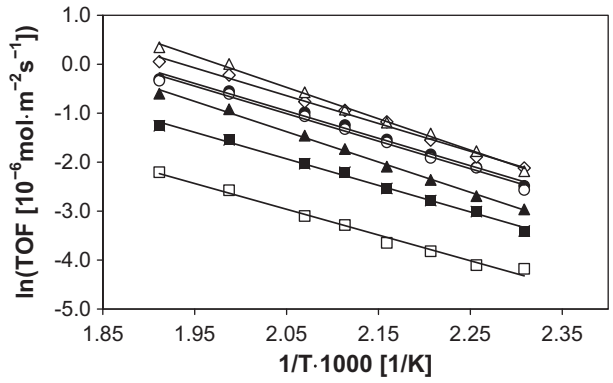

Fig. 2. Ln of TOF for uncoated copper catalysts between 160 and 250 °C (△ Cu/Al_2O_3-54, ◇ Cu/Al_2O_3-99, ♦ Cu/Al_2O_3-100, ● Cu/Al_2O_3-149, ○ Cu/Al_2O_3-151, ▲ Cu/Al_2O_3-214, ■ Cu/Al_2O_3-257 and □ Cu/Al_2O_3-360).

Table 2
Apparent energies of activation for the uncoated catalysts.

Catalyst	Apparent energy of activation (kJ mol^{-1})	Error (kJ mol^{-1})
Cu/Al_2O_3-54	53	±0.2
Cu/Al_2O_3-99	47	±0.2
Cu/Al_2O_3-100	50	±0.3
Cu/Al_2O_3-149	49	±0.1
Cu/Al_2O_3-151	49	±0.1
Cu/Al_2O_3-214	52	±0.2
Cu/Al_2O_3-257	45	±0.2
Cu/Al_2O_3-360	43	±0.6

reaction conditions used for the data reported in the literature (H_2 to CO ratio of ca. 5 and a CO_2 to CO ratio of 1.1). For this reason, we also compared our catalysts to a commercial low-temperature WGS catalyst (see Supplementary material).

On the basis of the turnover frequencies, the activity decreased with increasing surface area of the support, since the accessible copper surface area increased (*vide infra*). The variation of the particle size of the catalyst pointed the absence of interparticle diffusion limitations. A slight kinetic isotope effect was observed when D_2O was used instead of H_2O (see Supplementary material), leading to an approximately 16% lower rate of reaction.

3.2. Structural and electronic properties of uncoated catalysts

To determine the electronic structure of copper, the uncoated catalysts were reduced *in situ* at 250 °C and examined by X-ray absorption spectroscopy (XAS) as shown in Fig. 3. The fraction of oxidized Cu varied sympathetically with the specific surface area of the support. The degree of reduction of the Cu/Al_2O_3 catalysts was calculated from a linear combination of the XANES of Cu^0, Cu^I and Cu^{II} references (see Supplementary material), and it was found to vary between 95 and 66% (see Table 3).

The local environment of the Cu atoms with respect to the number of neighbors (N), the distance between them (r) and the statistical order (Debye-Waller factor σ^2) calculated from the EXAFS as well as the zero energy correction (E_0) are shown in Table 3. The particle size was determined from the average coordination number of the nearest metal neighbor atoms assuming a cuboctahedral geometry [28]. As indicated by XANES, the Cu–O concentration increases with increasing specific surface area.

A particle size of 1.1 nm for the Cu clusters, which can be related to a dispersion of 0.82, was determined for the catalysts with the highest activities in the low-temperature WGS reaction (Cu/Al_2O_3-149 and Cu/Al_2O_3-151). In contrast, the catalysts with the lowest activities either consisted of larger Cu particles (2.1 nm) not indicating oxygen neighboring atoms (Cu/Al_2O_3-54) or consisted of smaller copper clusters (0.7 nm) with a coordination number higher than 1 for oxygen neighbors (Cu/Al_2O_3-360).

3.3. Catalytic activity of ionic liquid coated copper catalysts

A comparison of turnover frequencies and the rate constants for the water–gas shift reaction between coated and uncoated catalysts is shown in Fig. 4. Catalysts based on Al_2O_3-54, Al_2O_3-149 and Al_2O_3-257 were tested. With increasing temperature, the turn over frequency of the coated catalysts decreased indicating a negative apparent energy of activation. We can exclude that this is only an effect of deactivation, as activity test for the coated catalysts at 160 and 200 °C indicated higher activity at the lower reaction temperature (see Supplementary material). (Note that we observed deactivation with time on stream, due to a sintering of the copper nanoparticles. Also, see the results from XAFS.)

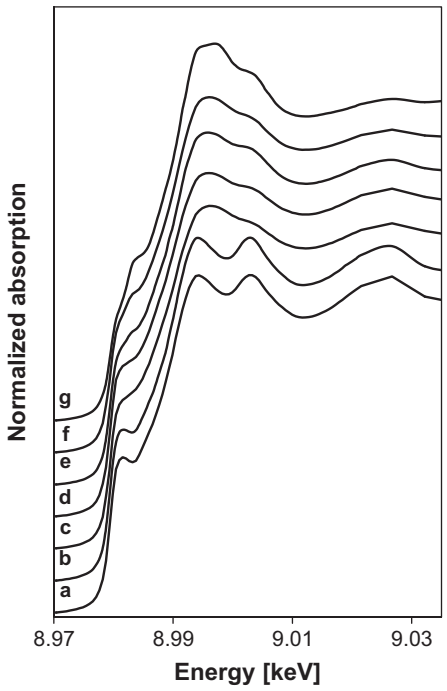

Fig. 3. XANES of uncoated copper catalysts ((a) Cu/Al_2O_3-54, (b) Cu/Al_2O_3-99, (c) Cu/Al_2O_3-149, (d) Cu/Al_2O_3-151, (e) Cu/Al_2O_3-214, (f) Cu/Al_2O_3-257 and (g) Cu/Al_2O_3-360.) after reduction at 250 °C.

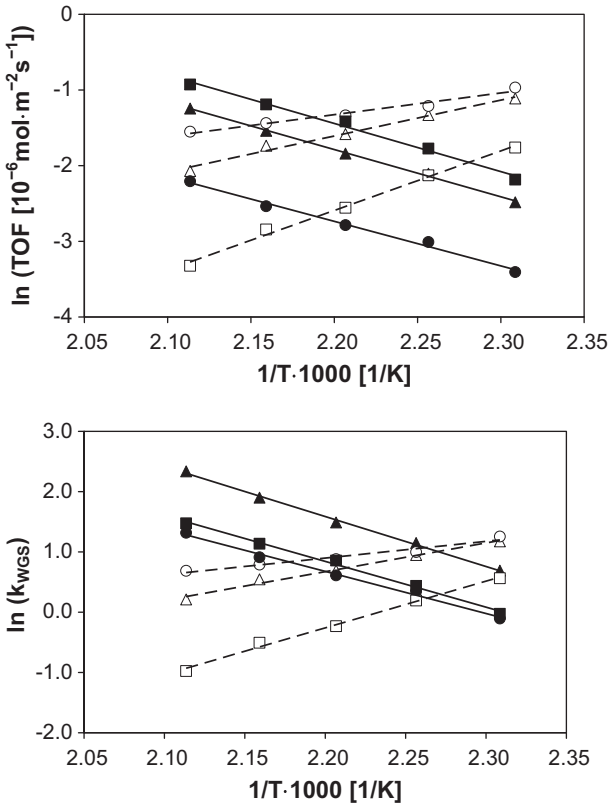

Fig. 4. Ln of TOF (upper part) and ln of rates (lower part) for ionic liquid coated (□ $Cu/BDiMIm/Al_2O_3$-54, △ $Cu/BDiMIm/Al_2O_3$-149, ○ $Cu/BDiMIm/Al_2O_3$-257) and uncoated (● Cu/Al_2O_3-257, ■ Cu/Al_2O_3-54, ▲ Cu/Al_2O_3-149) copper catalysts.

At lower temperatures (below 180 °C), the coated copper catalysts showed higher turnover frequencies as well as higher rate constants for the CO conversion compared to the uncoated catalysts. A comparison of the coated catalyst with the highest activity in the water–gas shift reaction ($Cu/BDiMIm/Al_2O_3$-257) and a commercial catalyst (ShiftMax-240) is given in Supplementary material. It is interesting to note that the coated catalyst was five times more active (on the basis of the TOF) at 160 °C, although the metal loading of the commercial catalyst was ten times higher.

3.4. Characterization of the electronic and structural properties of the ionic liquid coated catalysts under reaction conditions

The XANES collected during the reduction of an uncoated catalyst as well as of four BDiMIm coated (5, 10, 20 and 30 wt.%) copper catalysts in H_2 flow at 210 °C are complied in Fig. S7. In general, a higher concentration of ionic liquid present on the catalysts led to a higher degree of reduction of the Cu clusters, whereas for the uncoated catalyst XANES data indicates that the Cu particles are oxidized in part. Using a linear combination of the XANES of Cu^0 and Cu^I references for the quantitative analysis of the XANES structure, the average concentration of Cu^0 was determined to increase for example from 40% for the uncoated catalyst to 51%, 55%, 62% and 66% for the catalyst coated with 5, 10, 20 and 30 wt.% BDiMIm, respectively.

The catalysts used for the comparison of coated and uncoated systems (based on Al_2O_3-54, Al_2O_3-149 and Al_2O_3-257) were also examined by *in situ* XAS experiments. After the reduction of the catalyst at 215 °C, XAS was measured at liquid nitrogen temperature for the EXAFS analysis. Then, the sample was heated to 150 °C under He flow. Fig. 5 shows the spectra of Cu/Al_2O_3-149 in He at 150 °C, after dosing CO at 150 °C for 30 min, after 60 minutes under reaction conditions (CO to H_2O ratio 1:2) and in He after the reaction at 30 °C. When CO is added to the system, the oxidation state is lowered and a further reduction takes place when the sample is additionally exposed to water by the hydrogen generated. The structure of the copper nanoparticles after the reaction was determined by EXAFS analysis.

Table 3
Results from XAS analysis for uncoated copper catalysts after reduction at 250 °C.

	Al_2O_3-54	Al_2O_3-99	Al_2O_3-149	Al_2O_3-151	Al_2O_3-214	Al_2O_3-257	Al_2O_3-360
r_{CuO} (Å)	–	–	1.84	1.88	1.89	1.87	1.91
N_{Cu-O}	0	0	0.6	0.6	0.8	1.0	1.2
σ^2	–	–	0.003	0.004	0.003	0.005	0.004
E_0 (eV)	–	–	1.7	6.2	7.7	5.3	6.6
r_{CuCu} (Å)	2.53	2.53	2.53	2.53	2.53	2.53	2.53
N_{Cu-Cu}	9.4	9.2	7.1	7.0	6.0	5.8	5.5
σ^2	0.006	0.007	0.012	0.011	0.009	0.011	0.010
E_0 (eV)	4.5	4.4	2.8	3.4	2.6	1.5	3.6
Dispersion	0.56	0.59	0.81	0.82	0.89	0.90	0.92
Particle size (nm)	2.1	2.0	1.1	1.1	0.9	0.8	0.7
Degree of reduction (%)	95	91	83	84	76	72	66

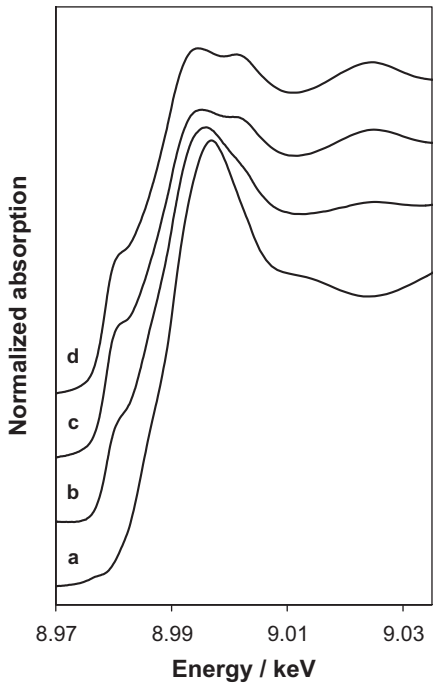

Fig. 5. XANES spectra of Cu/Al_2O_3-149 after reduction (a), in CO flow (b), under reaction conditions (c) and after reaction (d) (note that the catalysts were reduced at 215 °C before reaction and not at 250 °C as the catalysts shown in Fig. 3).

The averaged oxidation state of the coated catalysts after the reduction step is lower than for the uncoated systems. In presence of the reactants, the coated catalysts were also reduced, but the differences in the XAS are not as distinct as for the uncoated catalysts.

The XANES for the uncoated and coated catalysts after the reaction can be found in Supplementary material (Figs. S8 and S9). With Cu/Al_2O_3-149, the degree of reduction is higher compared to the other two tested uncoated supports. The XANES of the coated catalysts show the same oxidation state after treatment at reaction conditions and indicate an oxidation state closer to 0 (95% compared to 87%) than the uncoated catalysts.

The results of the EXAFS analysis before and after the treatment under reaction conditions are compiled in Table 4 (uncoated systems) and Table 5 (coated systems) (note that the catalysts were reduced at 215 °C before reaction and not at 250 °C as the catalysts shown in Table 3, leading to lower states of reduction).

For the uncoated catalysts, the number of copper–oxygen neighbors is reduced to 60–75% after and the treatment at reaction conditions, while the number of copper–copper neighbors increases indicating a sintering of the metal particles.

For the coated catalysts, copper–oxygen neighbors were not found after treatment at water–gas shift reaction conditions. The largest particles (d = 2.7 nm) after reaction can be found for the catalyst based on Al_2O_3-149. Note that the copper particle size was larger than with the uncoated catalysts.

3.5. Adsorption of CO, CO_2 and D_2O followed by IR spectroscopy

Adsorption of CO, CO_2 and D_2O was followed by IR spectroscopy in order to understand the interactions of the reactants with the active sites. Note that D_2O was used instead of H_2O to avoid absorption bands in the region of the perturbed OH vibrations resulting from the hydrogen bonding interaction between the OH groups of the support and ionic liquid [15].

The IR spectra of CO adsorbed on Cu/Al_2O_3 (a) and CO adsorbed on $Cu/BDiMIm/Al_2O_3$ (b) are shown in Fig. 6. For the uncoated catalyst, the adsorption of CO led to a band at 2088 cm^{-1} assigned to CO linearly adsorbed on Cu^0. For the coated catalyst, this band was smaller and shifted to 2117 cm^{-1}. In both cases, adsorbed CO was not observed after evacuation.

The adsorption of CO_2 on Cu/Al_2O_3 (shown in Fig. 7) led to bands at 1657 cm^{-1}, 1228 cm^{-1} (bridged bidentate carbonate),

Table 4
Results of EXAFS analysis for uncoated copper catalysts before and after reaction at 150 °C.

	Cu/Al_2O_3-54		Cu/Al_2O_3-149		Cu/Al_2O_3-257	
	before	after	before	after	before	after
r_{CuO} (Å)	1.97	1.97	1.91	1.92	1.91	1.95
N_{Cu-O}	0.8	0.6	1.0	0.6	1.1	0.6
σ^2	0.003	0.003	0.005	0.005	0.005	0.004
E_0 (eV)	21.4	13.8	8.6	8.8	9.8	12.1
r_{CuCu} (Å)	2.53	2.54	2.53	2.54	2.53	2.54
N_{Cu-Cu}	6.2	7.8	5.2	8.1	4.6	7.7
σ^2	0.008	0.006	0.009	0.007	0.010	0.007
E_0 (eV)	3.5	4.2	1.9	3.9	2.8	3.8
Dispersion	0.88	0.77	0.93	0.73	0.94	0.74
Particle diameter (nm)	0.9	1.3	0.7	1.4	0.6	1.2

Table 5
Results of EXAFS analysis for coated copper catalysts before and after reaction at 150 °C.

	$Cu/BDiMIm/Al_2O_3$-54		$Cu/BDiMIm/Al_2O_3$-149		$Cu/BDiMIm/Al_2O_3$-257	
	before	after	before	after	before	after
r_{CuO} (Å)	1.94	–	1.99	–	1.93	–
N_{Cu-O}	0.5	–	0.3	–	0.6	–
σ^2	0.006	–	0.001	–	0.006	–
E_0 (eV)	9.3	–	17.5	–	6.4	–
r_{CuCu} (Å)	2.54	2.54	2.54	2.54	2.54	2.54
N_{Cu-Cu}	9.0	9.7	9.4	10.0	9.0	9.7
σ^2	0.006	0.006	0.006	0.006	0.006	0.006
E_0 (eV)	4.8	4.6	5.2	4.6	4.9	4.1
Dispersion	0.63	0.51	0.54	0.46	0.63	0.51
Particle diameter (nm)	1.8	2.4	2.2	2.7	1.8	2.4

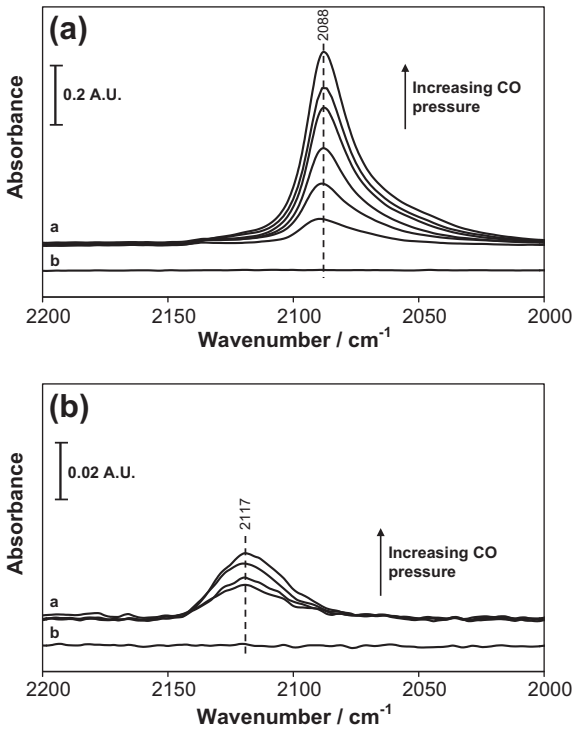

Fig. 6. IR absorption spectra of CO adsorbed on copper supported on alumina (a) and CO adsorbed on Cu/BDiMIm/Al_2O_3 (b) (spectrum b after evacuation).

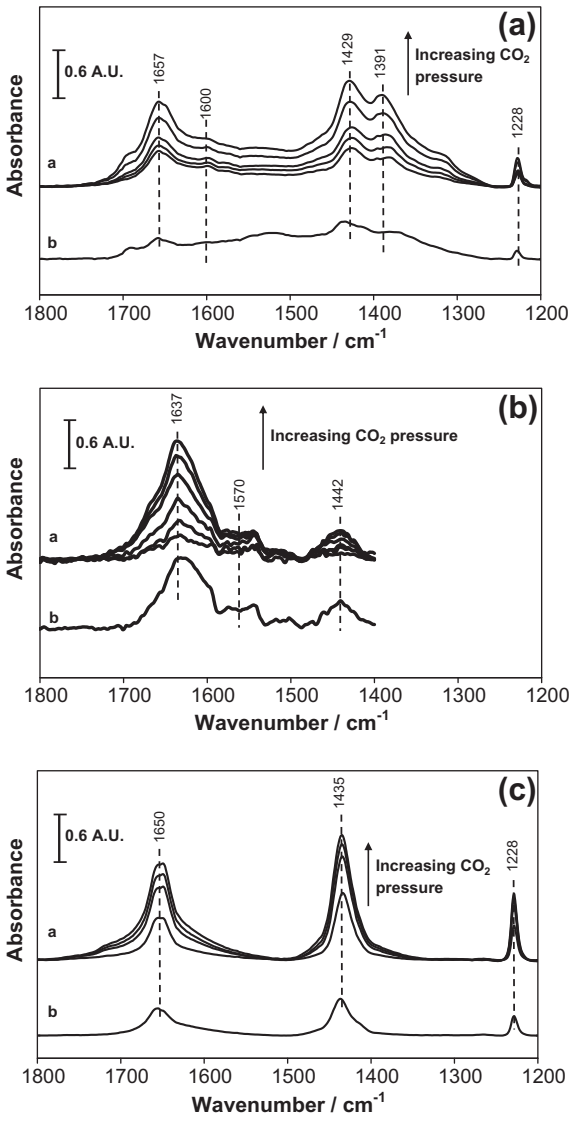

Fig. 7. IR absorption spectra of CO_2 adsorbed on copper supported on alumina (a), CO_2 adsorbed on Cu/BDiMIm/Al_2O_3 (b) and CO_2 adsorbed on Al_2O_3 (c) (spectrum b after evacuation) (please note that in (b) the region below 1400 cm^{-1} is not depicted, since the spectra would be dominated by changes of bands attributed to $CF_3SO_3^-$).

1429 cm^{-1} (ionic carbonate) and 1600 cm^{-1}, 1391 cm^{-1} (carboxyl). Bands characteristic for the formation of bridged bidentate carbonate (1637 cm^{-1}), carboxyl (1570 cm^{-1}) and an ionic carbonate species (1442 cm^{-1}) were only observed on Cu/BDiMIm/Al_2O_3. The region below 1400 cm^{-1} was dominated by changes of the absorption bands of the trifluoromethanesulfonate anion of the ionic liquid (*vide infra*). The concentration of CO_2 remaining on the sample after evacuation was higher for the coated catalyst. It should be noted that CO_2 was also adsorbed on the parent support. The observed bands were attributed to bridged bidentate carbonate species (1650 and 1228 cm^{-1}) and an ionic carbonate species at 1435 cm^{-1}.

Fig. 8 compiles the IR spectra after adsorption of D_2O. A broad band around 2570 cm^{-1} (symmetric and asymmetric stretching vibrations) with a feature at 2715 cm^{-1} (due to the formation of surface OD groups) for Cu/Al_2O_3 and around 2615 cm^{-1} for Cu/BDiMIm/Al_2O_3 was observed. (Note that due to hydrogen bonding, the bands for the symmetric and antisymmetric stretching vibrations were broadened resulting in only one band around 2570 cm^{-1} [29].) After evacuation, surface OD groups appeared at 2635, 2710 and 2745 cm^{-1} for the uncoated catalyst, and OD-hydrogen bonds were observed at 2625 cm^{-1} for the coated material. It should be noted that the maximum concentration of adsorbed D_2O was two times higher for Cu/BDiMIm/Al_2O_3. The adsorption of D_2O on Al_2O_3 showed identical result to the adsorption on Cu/Al_2O_3 indicating that the observed features are characteristic of adsorption on the support.

3.6. In situ infrared spectroscopy during reaction

Fig. 9 shows the surface species during the course of an experiment with an uncoated catalyst. After admitting CO at 150 °C the band at 2088 cm^{-1} indicated CO adsorbed on Cu^0. The concentration of adsorbed CO was reduced as soon as 10 vol.% water vapor was added to the reactant gas stream. The two bands appearing around 2330 and 2360 cm^{-1} correspond to CO_2 in the gas phase. The band at 1645 cm^{-1} is assigned to OH-bending vibrations of water. The band at 1574 cm^{-1} (appearing at temperatures higher than 170 °C) indicates a carboxyl species, and the bands at 1460 and 1420 cm^{-1} indicate the formation of monodentate and ionic carbonate species, respectively. With increasing temperature, the concentration of adsorbed CO and water was reduced, whereas the concentration of carbonates and gas phase CO_2 increased. Purging the catalysts with He at 150 °C after the reaction led to almost complete removal of adsorbed CO with a significant concentration of carbonates remaining on the surface.

Fig. 10 shows the difference IR spectra at reaction conditions for Cu/Al_2O_3-149, Cu/Al_2O_3-257 and Cu/Al_2O_3-54. (Note that the bands attributed to CO in the gas phase were subtracted from the spectra.) The position and intensity of the band assigned to CO on Cu^0 varies for the three catalysts. The smallest concentration of adsorbed CO was found for Cu/Al_2O_3-54 showing a band at 2110 cm^{-1}. With Cu/Al_2O_3-257, the band for monodentate CO was found at lower energy (2086 cm^{-1}) and an additional band

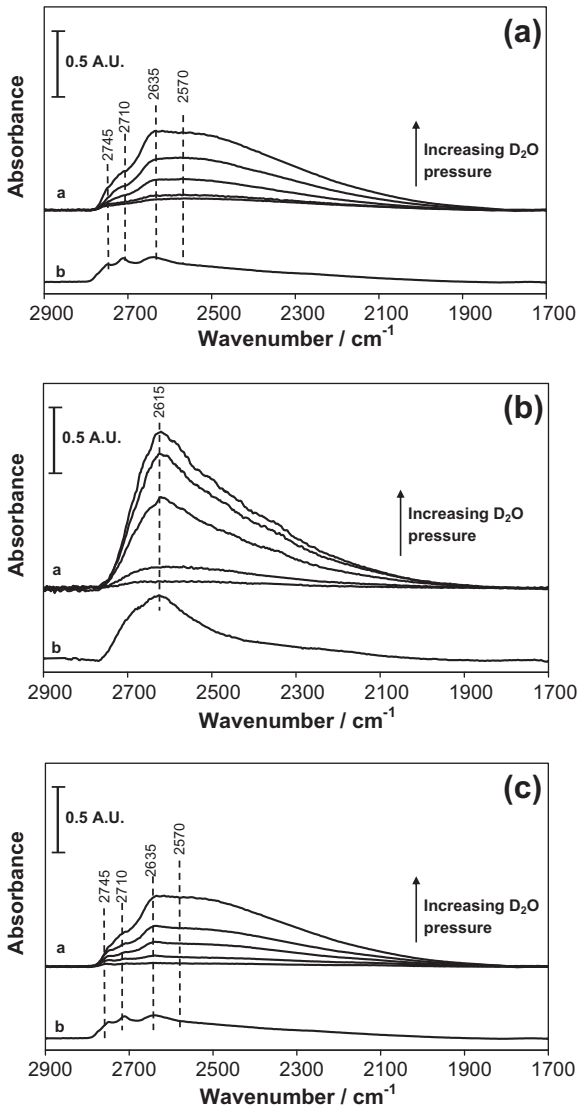

Fig. 8. IR absorption spectra of D_2O adsorbed on copper supported on alumina (a), D_2O adsorbed on Cu/BDiMIm/Al_2O_3 (b) and D_2O adsorbed on Al_2O_3 (c) (spectrum b after evacuation).

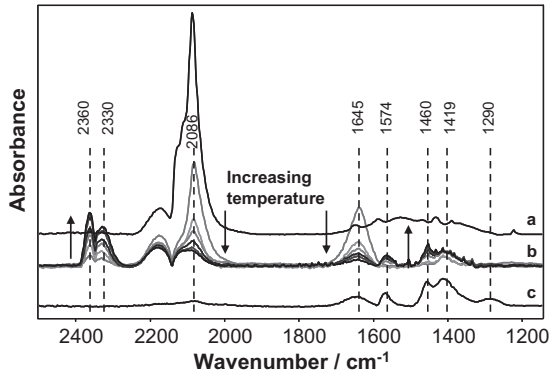

Fig. 9. Difference spectra of *in situ* IR experiment with uncoated Cu catalyst: 2.5 mL min^{-1} CO (a), temperature ramp with CO and water (b) and spectrum after exposure at reaction conditions (c).

at 2000 cm^{-1} was observed, which is attributed to CO adsorbed in a bridged mode. The intensity of the CO bands increased from Al_2O_3-54, over Cu/Al_2O_3-149 to Al_2O_3-257 with a ratio of 1:1.8:2.0. The intensity of the band attributed to the OH-bending remained constant for all three catalysts.

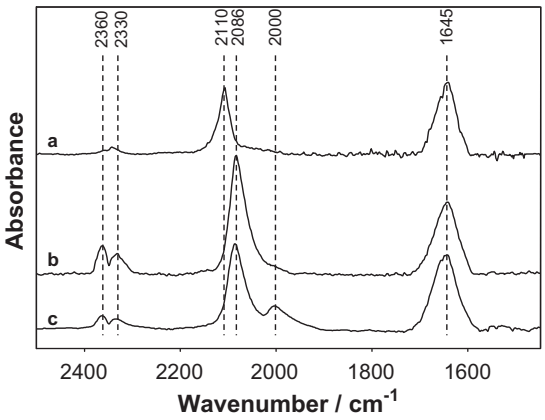

Fig. 10. Difference IR spectra at *in situ* conditions for Cu/Al_2O_3-54 (a), Cu/Al_2O_3-149 (b) and Cu/Al_2O_3-257 (c).

The comparison between the uncoated (Cu/Al_2O_3-149) and a coated sample (Cu/BDiMIm/Al_2O_3-149), shown in Fig. 11, indicates that only a small concentration of CO is adsorbed on the surface of the ionic liquid coated catalyst (when purging with He the band at 2110 cm^{-1} results from CO adsorbed on Cu). It should, however, be emphasized that also the intensity of the band for OH-bending vibrations of molecular water is smaller for the coated catalyst. The bands at 1485 and 1570 cm^{-1}, observed only on the coated catalyst, indicate the formation of carbonate and carboxyl species on Cu/BDiMIm/Al_2O_3-149. Also, experiments with Cu/BDiMIm/Al_2O_3-54 and Cu/BDiMIm/Al_2O_3-257 were performed. It was observed that the band attributed to antisymmetric SO_3 stretching of trifluoromethanesulfonate (the anion of the ionic liquid) ion pairs was increased for Cu/BDiMIm/Al_2O_3-257 under reaction conditions (also see the following remarks on the interactions of the reactants with anion of the ionic liquid). In contrast to the uncoated catalyst, the intensity (20% for Cu/BDiMIm/Al_2O_3-149 and 30% for Cu/BDiMIm/Al_2O_3-257) of the band attributed to the OH-bending vibrations increases with surface area for the coated catalysts.

To investigate the influence of the reactants on the ionic liquid, the absorption region of the trifluoromethanesulfonate anion of two samples with a ionic liquid coating of 5 and 20 wt.% is compared in Figs. S10 and S11, respectively. In both cases, the IR

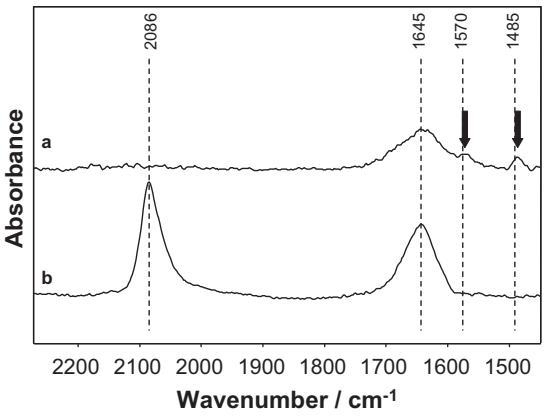

Fig. 11. Comparison of the difference spectra of a coated (a) and an uncoated (b) copper catalyst.

spectra before reduction, after reduction, in a flow of CO, at reaction conditions (10% water) and after reaction are displayed.

For the catalyst with a loading of 5 wt.% ionic liquid, bands were observed at 1171 cm^{-1} (antisymmetric CF_3), 1225 cm^{-1} (symmetric CF_3), 1242 cm^{-1} (antisymmetric SO_3 stretching of trifluoromethanesulfonate ion pairs) and 1275 cm^{-1} (antisymmetric SO_3 deformation vibrations). After reduction of the catalyst, the bands attributed to the antisymmetric SO_3 stretching of trifluoromethanesulfonate ion pairs and to the antisymmetric SO_3 deformation vibrations decreased in intensity, and a new band was observed at 1330 cm^{-1}. At the same time, the bands attributed to CF_3 vibrations were shifted to lower wavenumbers. Upon flowing CO over the catalyst, only small changes were observed in the spectrum, but after adding water the spectrum changed appeared to be very similar to the spectrum before reduction. This indicates that the presence of water seems also to induce changes in the interaction of the ionic liquid with the metal surface.

The spectra of the catalyst with an ionic liquid loading of 20 wt.% showed four bands before admission of H_2. Antisymmetric and symmetric CF_3 vibrations were observed at 1154 cm^{-1} and at 1222 cm^{-1}, the antisymmetric SO_3 stretching of trifluoromethanesulfonate ion pairs and the antisymmetric SO_3 deformation vibrations at 1240 and 1275 cm^{-1}. A band at 1330 cm^{-1} appeared again after reduction and disappeared after exposing the catalyst to CO/H_2O. In contrast to the catalyst with the lower loading, the other parts of the spectra were hardly influenced by changing the gas atmosphere.

The spectra of the catalyst with a higher loading of ionic liquid imply that only the direct interaction with the surface can be observed. The changes of the oxidation state of copper and the interaction of the surface species with the ionic liquid can only be observed by the appearance and disappearance of the band at 1330 cm^{-1}. The changes of the other bands are overlaid by the vibrations of molecules in the bulk phase.

4. Discussion

4.1. State of the catalysts

XANES indicated that the fraction of oxidized Cu in the uncoated catalysts increased in parallel to the specific surface area of the support. Cu/Al_2O_3-54 and Cu/Al_2O_3-99 were nearly fully reduced, while a significant fraction of oxidized Cu was observed with the other catalysts. In line with the increase in the white line, EXAFS showed that the number of oxygen neighbors increased in parallel to the surface area of the support confirming the presence of a higher fraction of oxidized Cu. As the copper particles size decreased with increasing specific surface area of the support, the results show that the fraction of oxidized Cu increases, as the particle size decreases.

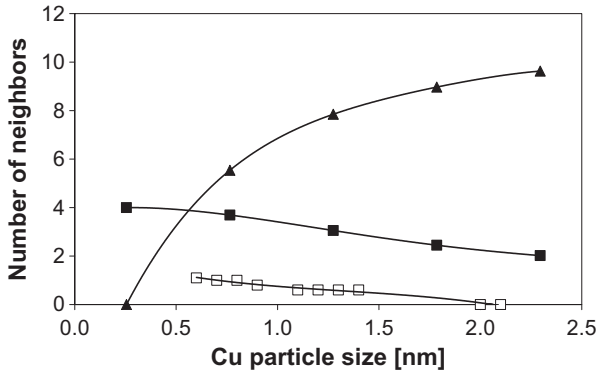

Fig. 12. Calculated maximum number of copper (▲) and oxygen neighbors (■) assuming cuboctahedral geometry and the observed numbers of neighbors for oxygen (□) in dependence of copper particle size (oxygen is only located on the surface of the catalyst).

Because the Cu–Cu distances in the particles were identical with those of metallic Cu, the oxygen atoms are concluded to be located at the surface of the copper particles. Fig. 12 shows the maximum number of oxygen neighbors possible at the surface assuming that the oxygen atoms are located in the tetrahedral and octahedral vacancies of the copper surface. A visualization of the location of O on the surface of Cu(1 1 1) and (1 0 0) terminated particles are shown in Fig. 13. A cluster containing 147 Cu atoms has 6 (1 0 0) and 8 (1 1 1) surfaces with 16 and 10 Cu atoms on each surface, respectively. On each (1 0 0) surface 9 oxygen atoms can be coordinated to the vacancies, whereas for the (1 1 1) surfaces a maximum of six oxygen atoms can be coordinated leading to 102 oxygen atoms that can be coordinated to a Cu cluster with

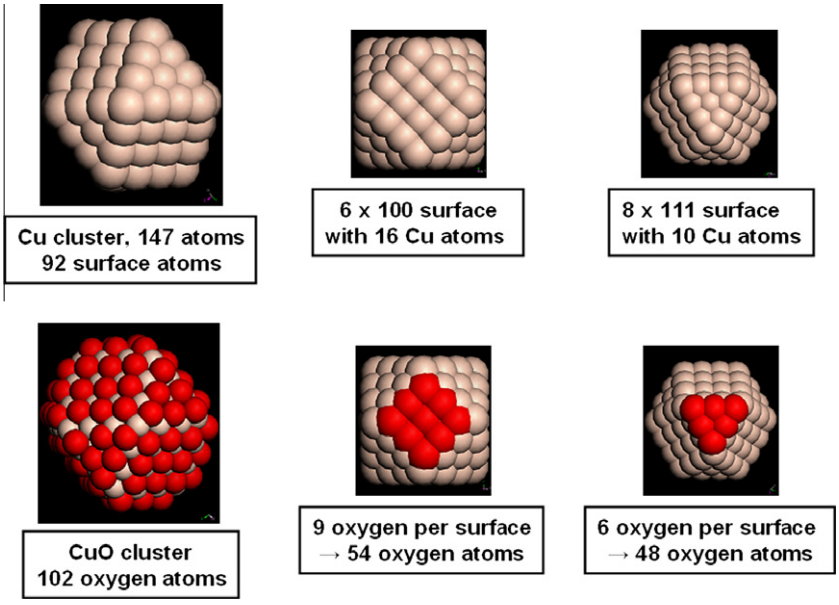

Fig. 13. Model of ideal cuboctahedral Cu cluster with oxygen atoms in tetrahedral and octahedral vacancies.

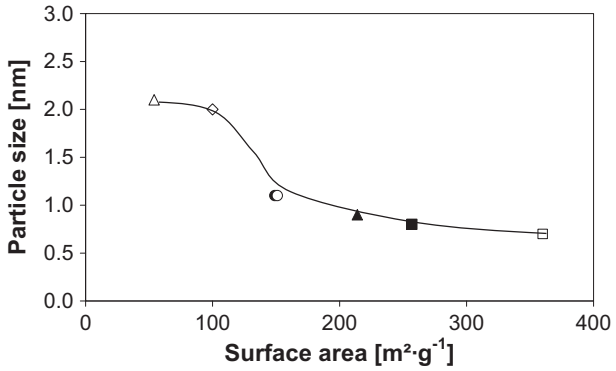

Fig. 14. Particle size in dependence of support surface area (□ Cu/Al_2O_3-360, ■ Cu/Al_2O_3-257, ▲ Cu/Al_2O_3-214, ● Cu/Al_2O_3-149, ○ Cu/Al_2O_3-151, ◇ Cu/Al_2O_3-99 and △ Cu/Al_2O_3-54).

147 atoms. This results in a maximum number of oxygen neighbors of 2.5 and a Cu–Cu coordination number is 9.0. For a given copper particle size, the number of oxygen neighbors found experimentally were 20–30% of the theoretically determined maximum coordination numbers. Thus, we conclude that at most about one-third of the copper surface atoms were blocked by oxygen. It should be noted at this point that oxygen on the copper surface plays an important role for the structure the nanoparticles adopt, if exposed to water–gas shift conditions (*vide infra*).

Because the fraction of the potential interface between the metal particle and the oxide support is much smaller than the fraction of the oxidized Cu, we conclude the oxygen atoms on the surface are located to a large extent on the accessible part of the copper nanoparticles. Please note that accessible copper surface area was estimated from the results of the EXAFS analysis, which perfectly agreed with the N_2O chemisorption experiments. (Results are presented in Supplementary material.)

The presence of large copper particles observed for supports with a lower specific surface area (see Fig. 14) is attributed to the fact that during the preparation procedure the local concentration of the copper ions is higher in the case of a low surface area support (8.8 Cu^{2+} per nm^2) compared to a high surface area support (1.3 Cu^{2+} per nm^2). This facilitates agglomeration of the precursor or the metal atoms in formation process.

Compared to the uncoated catalysts, the IL-coated catalysts show a higher degree of Cu reduction after treatment in hydrogen. As the concentration of the supported ionic liquid increases, the fraction of metallic Cu increased. This is attributed to the high solubility of water, formed during reduction as well as the low solubility of oxygen in the polar ionic liquid. With the coated catalysts also the copper particle size was higher than with uncoated catalysts (see Table 2). It indicates that the ionic liquid increases either the mobility of the precursor salt or the mobility of the Cu particles as they are formed indicating that the restructuring of nanoparticles is facilitated by the ionic liquid.

Also, the observed Cu–O distances for the coated and uncoated samples correlate perfectly with the degree of oxidation, as a large distance is found for the more oxidized samples. Note that the Cu–O distance in Cu_2O is around 1.85 Å, whereas the distance in CuO is 1.95 Å.

4.2. Sorption of reactants

For the uncoated catalysts, the *in situ* IR spectra reflect the different size of the copper particles. The wavenumber of the band attributed to CO adsorbed on Cu^0 was shifted from 2082 cm^{-1} (Cu/Al_2O_3-149) to 2110 cm^{-1} (Cu/Al_2O_3-54). As the fraction of oxygen on the Cu surface is lower on the larger particles than on the smaller, the increase in wavenumber of adsorbed CO indicates stronger dipole–dipole interactions of CO adsorbed on larger particles. However, we cannot rule out strong bonding on defect sites of the smaller particles. This is supported by the fact that for the Cu/Al_2O_3-257 catalyst bridged bonded CO was found indicating an even stronger bond to the surface compared to the other catalysts. Note that this is in good agreement with the fact that the observed apparent energy of activation was lower for the catalyst with the highest surface area. Corrected for the number of free accessible surface atoms of Cu, the concentration of adsorbed CO was identical on all three samples investigated (see Supplementary material). The linear correlation passes, however, not through the origin indicating that a certain constant fraction of the reduced Cu is blocked by other species or is not accessible for CO, e.g., the interface between the particle and the support.

In addition to the bands of bridged bidentate carbonates and ionic carbonates, which were also observed with the parent support, carboxylic species were observed on the uncoated copper catalyst indicating that in the presence of carbon–metal bonds. As this carboxyl species is also observed in the *in situ* experiments, we conclude that the reaction involves the formation of $^*COOH$ group on the surface, which is a strong indication that the reaction follows the associative mechanism [5,11].

Because the IR spectra after of D_2O on the uncoated copper catalyst and the parent support were identical, we conclude that water is adsorbed in its majority on the support and that the adsorption is not influenced by the relatively small concentration of copper nanoparticles. However, water must also adsorb on the Cu particles, as its dissociation on Cu is the prerequisite for the catalytic chemistry. Because the dissociation of water, which is facilitated by the presence of adsorbed oxygen [30], is generally considered to be the rate-determining step, the concentration of OH groups on Cu is assumed to be small.

With coated catalysts, the band of adsorbed CO on Cu covered with IL at 2117 cm^{-1} appeared at higher wavenumber than the corresponding band with uncovered Cu particles. The lower coverage in the case of IL covered Cu particles (in line with the low activity of CO dissolved in the ionic liquid in accordance with the literature [31–33]) allows us to exclude CO dipole coupling as cause for this blue shift. Because the oxygen coverage of the IL covered particles after reduction with H_2 at 215 °C is minimal (judged from the XAFS data), the blue shift is tentatively attributed to markedly weakened CO adsorption in the presence of the ionic liquid due to the competitive interaction of the ionic liquid with the Cu surface.

While the concentration of CO_2 adsorbed was higher for the coated catalyst after evacuation, the principal states of adsorbed CO_2 on the uncoated and coated catalysts were concluded to be identical. The downward shift of the bands of the bridged bidentate carbonate and carboxylic species together with the changes in the bands of the trifluoromethanesulfonate species with the coated catalyst results from the interaction of the ionic liquid with chemisorbed CO_2. The higher concentration of bidentate carbonate indicates that chemisorbed CO_2 is stabilized by the ionic liquid, which is in good agreement with the strong interaction of CO_2 with the CF_3-group (*vide infra*) [34–36].

D_2O adsorption showed that the concentration of adsorbed water was two times higher for the coated catalyst, because the ionic liquid [37] increases the activity of water during the water–gas shift reaction. It is interesting to note that despite the stronger interactions, the IR stretching band of adsorbed water was broader in the case of the uncoated catalyst than with the IL covered samples indicating a less diverse environment in the latter case.

The strong interactions between the reactants and the ionic liquid are also reflected in the changes of the IR bands of the IL

$CF_3SO_3^-$ groups. Note that mainly the anion of the ionic liquid is interacting with the surface [15]. The change from $Cu^{I/II}$ to Cu^0 after the reduction leads to a decrease of the band at 1275 cm^{-1} attributed to antisymmetric sulfonate vibration and the appearance of a band at 1330 cm^{-1} attributed to this vibration of a species with a stronger S═O bond. This increases the bond strength of two sulfonate oxygen atoms with the surface, which in turn increases the strength to the remaining bonds to the oxygen and the carbon atom. Indeed, the bands corresponding to CF_3 vibrations are shifted to lower wavenumbers indicating weaker C—F bonds as electrons from Cu^0 are pushed into the CF_3 antibonding σ^* orbital [38]. Thus, we conclude that the trifluoromethanesulfonate is adsorbed sideways and normal to the surface with two oxygen atoms bound to Cu. After admitting CO and water, however, the spectrum turned back to its state before reduction indicating that the interaction of CO with Cu is stronger (despite its reduced strength in the presence of the IL) than the interaction with $CF_3SO_3^-$.

4.3. Water–gas shift catalysis

For the uncoated catalysts, the highest rate (per gram catalyst) in the low-temperature water–gas shift reaction was observed for Cu supported on both Al_2O_3-149 and Al_2O_3-151 with a fraction of about 20% of the Cu atoms being oxidized. Fig. 15 shows that the rate decreases with higher and with lower degrees of reduction. The copper particle size for these catalysts determined from EXAFS was 1.1 nm and in average 0.6 oxygen neighbors for the Cu atoms were observed (compared to maximally 3.3 oxygen neighbors if the entire surface of the cluster is occupied with oxygen).

While we have used a comparison of the rate constants to evaluate the performance of the catalysts (all catalysts had the same copper loading), we would also like to address the influence the accessible copper surface area on the activity. The turnover frequencies for the five uncoated catalysts are compared in Fig. 16, which shows that the TOF decreases with increasing support surface area. The degree of reduction and also the particle size increased during the treatment of the materials with CO and during the water–gas shift reaction. XANES shows that the degree of reduction increases after flowing CO over the catalyst for 30 min. Under these conditions, the formation of bidentate CO species can be observed by IR spectroscopy, which can be related to a change of the shape of the nanoparticles induced by the reaction of CO with surface oxygen. It is also remarkable that Cu is further reduced by admission of water to the stream of CO, which can be attributed to the oxygen aided dissociation of water forming two hydroxyl groups quickly reacting with adsorbed CO to carboxylic surface species. The fact, that the size of the copper particles as well as the number of oxygen neighbors was similar for all uncoated samples after reaction, (note that the catalytic activity was different) implies that not only the size of the clusters is of importance for the reactivity, but it also suggests that the structure of the nanoparticles and the concentration of highly uncoordinated sites are important. Note in this respect that copper nanoparticles containing defect sites are claimed to lead to a higher CO conversion activity [39]. Thus, it appears that the structure of the copper particles before the reaction determines the reactivity of the catalysts. In this context, we speculate that for the catalysts having a high fraction of metallic Cu (Cu/Al_2O_3-99 and Cu/Al_2O_3-54) less defect sites can be formed by removing oxygen leading to less active catalysts. For the nanoparticles itself, the turnover frequency decreased with the particle size. IR spectroscopy indicated that the smaller particles interact stronger with CO (see the formation of bidentate CO in Fig. 10c), which blocks the metal sites for further reaction.

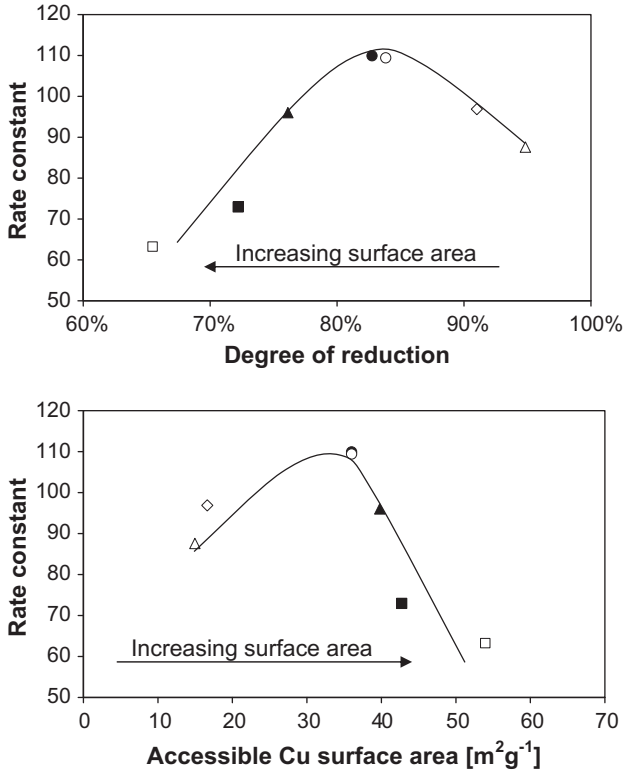

Fig. 15. Activity of uncoated copper catalysts in dependence of the degree of reduction (upper part) and in dependence of accessible Cu surface area (lower part) (□ Cu/Al_2O_3-360, ■ Cu/Al_2O_3-257, ▲ Cu/Al_2O_3-214, ● Cu/Al_2O_3-149, ○ Cu/Al_2O_3-151, ◇ Cu/Al_2O_3-99 and △ Cu/Al_2O_3-54).

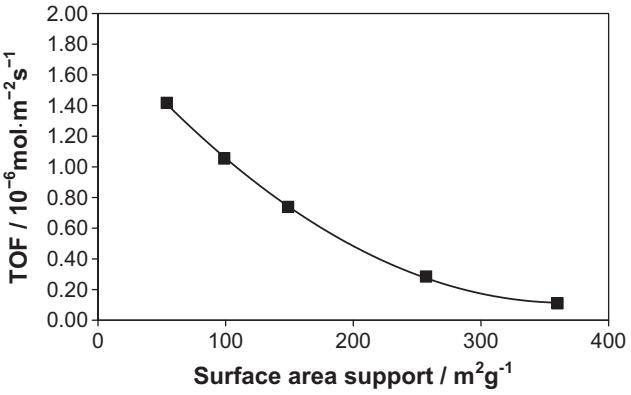

Fig. 16. TOF (mol CO per m^2 of accessible Cu) in dependence of the support surface area.

A kinetic isotope effect (k_H/k_D) of 1.2 was observed for the uncoated catalyst. This confirms that the steps of the reaction mechanism involving an abstraction of hydrogen (abstraction of hydrogen from water and the decomposition of $^*COOH$) are involved in the rate-determining step.

To compare the activities of coated and uncoated catalysts three catalysts were chosen, i.e., Cu/Al_2O_3-54, Cu/Al_2O_3-149 and Cu/Al_2O_3-257, being examples for the optimum catalyst state as well as one for a too high and one for a too low degree of reduction for the uncoated materials. In case of the coated catalysts, however, XAFS confirmed that the oxidation state and the copper particle size of all catalysts were similar. The catalytic activity increased with increasing specific surface area of the support leading to a lower averaged thickness of the IL film. On the one hand, this leads to changes in the interactions of the ionic liquid with the reactants. Also, the amount of dissociated water on the surface of the catalyst

was higher for the materials with a thinner film. This can be explained by the fact that the concentration of water near to the surface was higher compared to the materials with a thicker film, where the water molecules are distributed throughout the film.

At temperatures below 180 °C, the coated catalysts were more active than the uncoated materials. Due to the higher activity, the formation of carboxyl species was observed at lower temperatures compared to the uncoated systems, also indicating that these species are stabilized by the ionic liquid. With increasing temperatures, the catalytic activity for the coated catalysts decreased leading to an apparent negative energy of activation. We tentatively attributed this to the decreasing solubility of the reactants in the ionic liquid with increasing temperatures. IR experiments showed that the concentration of adsorbed CO at higher temperatures is more reduced for the coated compared to the uncoated catalysts. Note that also the enhanced particle growth for the coated catalysts can be accounted for the lower activity at higher temperatures.

The question arises at this point as to why the coated catalysts are more active than the uncoated ones and why the activity drops with increasing reaction temperature. The activity of catalysts in the water–gas shift reaction is determined by the concentration of the reactants at the active sites and by the intrinsic activity of the catalyzing metal. Because the coated catalysts have an environment different from the gas phase at the surface, also the concentrations/activities of the educts in the ionic liquid have to be considered. This is especially important for CO, as the solubility of CO in ionic liquids is known to be low [32].

At equilibrium conditions, Henry's law can be applied to determine the activity of CO in the ionic liquid:

$$K_{H,CO}(T,p)\cdot a_{CO}(T,m_{CO}) = f_{CO}(T,p) \tag{7}$$

with Henry's constant of CO in the ionic liquid $k_{H,CO}(T,p)$, the activity of CO in the ionic liquid $a_{CO}(T,m_{CO})$ and the fugacity of CO in the vapor phase $f_{CO}(T,p)$. $k_{H,CO}$ in the supported ionic liquid is 54 MPa (determined from CO adsorption experiments on coated catalysts with and without copper, see Supplementary material). This is in excellent agreement with the published value of $k_{H,CO}$ (55 MPa) [32]. Note that the presence of copper increases the CO uptake by a factor of 30, due to the interaction of CO with copper.

The dependence of the chemical potential of CO on the fugacity of CO is given by:

$$\mu_{CO_{gas}} = \mu^{og} + RT\cdot\ln(f_{CO}/p^{o}) \tag{8}$$

with the fugacity dependent chemical potential μ_{COgas}, the standard chemical potential of CO in the gas phase μ^{og} (−137 kJ/mol [40]), the general gas constant R, the temperature T and the standard pressure p^o.

When dissolved in the ionic liquid the chemical potential of CO changes to:

$$\mu_{COsol} = \mu^{os} + RT\cdot\ln(a_{CO}(T,m_{CO})) \tag{9}$$

with the standard chemical potential of CO in the fluid phase μ^{os}.

At equilibrium conditions, ($\Delta G = \Sigma_i \nu_i \cdot \mu_i = 0$) μ_{COgas} is equal to μ_{COsol}. Thus, by combining Eqs. (7)–(9), μ^{os} can be calculated to be −122 kJ/mol for the supported ionic liquid. By comparison μ_{COsol} with μ^{og} (see Fig. 17), the activity of CO at equilibrium conditions is $a_{CO}(T, m_{CO}) = 0.002$ for the supported ionic liquid.

This shows that as expected the activity of CO in the supported ionic liquid is low, in perfect agreement with the results obtained by IR spectroscopy. The concentration of adsorbed CO is, thus, reduced to approximately 4%, when the catalyst is coated with ionic liquid.

The same considerations can be made for H_2O. Using $k_{H,H2O}(T, p) = 0.05$ [41] and $\mu^{og} = -228$ kJ/mol [42], μ^{os} can be calculated to

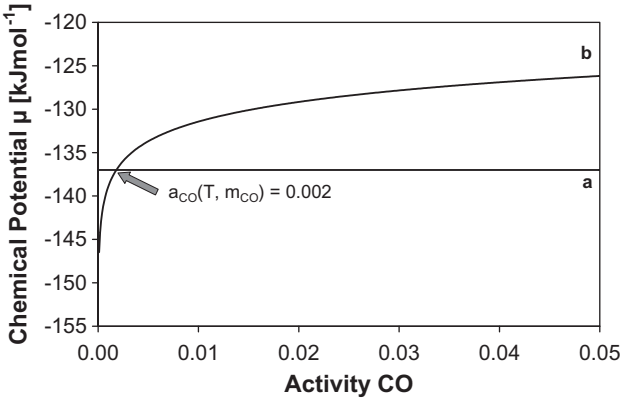

Fig. 17. Chemical potential of CO in the vapor phase (a) and of CO dissolved in a supported ionic liquid (b).

−230 kJ/mol indicating that 2.75 times more water than copper is present at equilibrium conditions. This is also in good agreement with the IR results, as the amount of observed adsorbed water two times higher for the coated catalyst, due to the interactions of the water molecules with the ionic liquid [37]. As pointed out earlier, the energetic barrier to abstract an H from H_2O is about seven times higher than the barrier to desorb water from the catalyst surface [5], therefore, the increased concentration of water adjacent to the active sites will lead to a higher rate since the probability to cleave the O—H bond is higher.

Not only the interaction of H_2O, but also the interaction of the intermediate carboxyl species with the ionic liquid benefits the reaction, because the decomposition of *COOH (abstraction of H from *COOH) is the second high energy barrier of the water–gas shift reaction. As the ionic liquid interacts with CO_2 [34–36], it is conceivable that also these carboxyl species interact with the ionic liquid and facilitate the abstraction of hydrogen. Formate species, formed from CO_2 and H, are assumed to block the active sites and can reach considerable surface coverages [5]. The presence of the ionic liquid weakens their adsorption strength leading to less blocked active sites.

Consequently, the presence of the IL leads to a higher concentration of the reacting species by weakening of all interactions with the surface and at the same time by adjusting the activities in the liquid phase above the catalyst. A higher concentration of oxygen facilitates the dissociation of water, but as the oxygen concentration increases the concentration of adsorbed CO must decrease creating so a maximum in activity for catalysts with alumina supports of intermediate specific surface area.

5. Conclusions

The detailed characterization by *in situ* spectroscopy methods of the interactions of ionic liquids with supported metal nanoparticles leads to detailed insight into the reactivity of the catalysts in the low-temperature water–gas shift reaction.

The copper particle size and, thus, the reduction degree vary sympathetically with the specific surface area of the support. The copper particle sizes as well as the fraction of unreduced Cu and of adsorbed oxygen atoms determine the catalytic activity in the water–gas shift reaction. Overall, the TOF of the water–gas shift increases with decreasing particle size. The presence of adsorbed oxygen on the one hand increases the rate as it reduces the barrier for water dissociation. At the same time, the surface coverage with CO increases. If CO is bound too weakly (Cu/Al_2O_3-54) or too strongly (Cu/Al_2O_3-257) to the active site, the reactivity in the water–gas shift reaction is decreased. In the former case, the water

adsorption is more difficult on the nearly oxygen-free catalysts, while on the oxygen-rich materials the strong interaction with CO leads to a lower concentration of water. In the presence of the IL, CO is adsorbed weakly improving the competitiveness for the adsorption of water.

Catalysts coated with the ionic liquid showed a higher turn over frequency for the water–gas shift reaction at low temperatures compared to uncoated and commercial systems. This is attributed due to a higher concentration of water in the proximity of the active sites and due to the interaction of the ionic liquid with reaction carboxyl intermediates facilitating the decomposition of these species. The observed concentrations of the reactants on the ionic liquid coated catalysts are in good agreement with this interpretation.

The present results indicate potential to develop easily manageable and highly active catalysts with a lower metal loading for low-temperature water–gas shift superior in activity to the present commercial systems.

Acknowledgements

The project is funded by the BMBF (promotional reference 03X2012F). The authors are grateful to Max-Buchner-Stiftung for partial support. The authors acknowledge fruitful discussions in the framework of the network of excellence IDECAT. The authors would like to thank HASYLAB, Hamburg, Germany and the ESRF in Grenoble, France for providing beam time at station X1 and BM26 for XAFS experiments. Xaver Hecht and Martin Neukamm are thanked for the experimental support. Furthermore Solvent Innovation GmbH and Süd Chemie AG are acknowledged for providing chemicals.

Appendix A. Supplementary material

Supplementary data associated with this article can be found, in the online version, at doi:10.1016/j.jcat.2010.09.019.

References

[1] D.L. Trimm, Appl. Catal., A 296 (2005) 1.
[2] Y. Amenomiya, G. Pleizier, J. Catal. 76 (1982) 345.
[3] T.M. Yureva, Kinet. Catal. 10 (1969) 862.
[4] J.A. Rodriguez, P. Liu, J. Hrbek, J. Evans, M. Perez, Angew. Chem., Int. Ed. 46 (2007) 1329.
[5] A.A. Gokhale, J.A. Dumesic, M. Mavrikakis, J. Am. Chem. Soc. 130 (2008) 1402.
[6] T. Shido, Y. Iwasawa, J. Catal. 140 (1993) 575.
[7] C.V. Ovesen, P. Stoltze, J.K. Norskov, C.T. Campbell, J. Catal. 134 (1992) 445.
[8] C.V. Ovesen, B.S. Clausen, B.S. Hammershoi, G. Steffensen, T. Askgaard, I. Chorkendorff, J.K. Norskov, P.B. Rasmussen, P. Stoltze, P. Taylor, J. Catal. 158 (1996) 170.
[9] P.B. Rasmussen, P.M. Holmblad, T. Askgaard, C.V. Ovesen, P. Stoltze, J.K. Norskov, I. Chorkendorff, Catal. Lett. 26 (1994) 373.
[10] G.C. Wang, L. Jiang, Z.S. Cai, Y.M. Pan, X.Z. Zhao, W. Huang, K.C. Xie, Y.W. Li, Y.H. Sun, B. Zhong, J. Phys. Chem. B 107 (2003) 557.
[11] Q.L. Tang, Z.X. Chen, X. He, Surf. Sci. 603 (2009) 2138.
[12] A. Riisager, R. Fehrmann, S. Flicker, R. van Hal, M. Haumann, P. Wasserscheid, Angew. Chem., Int. Ed. 44 (2005) 815.
[13] O. Jimenez, T.E. Muller, C. Sievers, A. Spirkl, J.A. Lercher, Chem. Commun. 2974 (2006).
[14] C. Sievers, O. Jimenez, R. Knapp, X. Lin, T.E. Muller, A. Turler, B. Wierczinski, J.A. Lercher, J. Mol. Catal. A: Chem. 279 (2008) 187.
[15] R. Knapp, A. Jentys, J.A. Lercher, Green Chem. 11 (2009) 656.
[16] C.P. Mehnert, E.J. Mozeleski, R.A. Cook, Chem. Commun. 3010 (2002).
[17] T. Welton, Coord. Chem. Rev. 248 (2004) 2459.
[18] R. Atkin, G.G. Warr, J. Am. Chem. Soc. 127 (2005) 11940.
[19] C. Sievers, O. Jimenez, T.E. Muller, S. Steuernagel, J.A. Lercher, J. Am. Chem. Soc. 128 (2006) 13990.
[20] A. Wolfson, I.F.J. Vankelecom, P.A. Jacobs, Tetrahedron Lett. 44 (2003) 1195.
[21] H. Hagiwara, Y. Sugawara, K. Isobe, T. Hoshi, T. Suzuki, Org. Lett. 6 (2004) 2325.
[22] S.M. Webb, Phys. Scripta T115 (2005) 1011.
[23] A.L. Ankudinov, B. Ravel, J.J. Rehr, S.D. Conradson, Phys. Rev. B 58 (1998) 7565.
[24] A.L. Ankudinov, J.J. Rehr, Phys. Rev. B 62 (2000) 2437.
[25] K.V. Klementiev, XANES Dactyloscope, Freeware: <http://www.desy.de/~klmn/xanda.html>.
[26] O. Hinrichsen, T. Genger, M. Muhler, Chem. Eng. Technol. 23 (2000) 956.
[27] N.A. Koryabkina, A.A. Phatak, W.F. Ruettinger, R.J. Farrauto, F.H. Ribeiro, J. Catal. 217 (2003) 233.
[28] R.E. Benfield, J. Chem. Soc., Faraday Trans. 88 (1992) 1107.
[29] B. Redlich, Ph.D. Thesis, Universität Hannover (Hannover), 1998.
[30] G.C. Wang, S.X. Tao, X.H. Bu, J. Catal. 244 (2006) 10.
[31] J. Jacquemin, P. Husson, V. Majer, M.F.C. Gomes, Fluid Phase Equilib. 240 (2006) 87.
[32] J. Kumelan, A.P.S. Kamps, D. Tuma, G. Maurer, Fluid Phase Equilib. 228 (2005) 207.
[33] I. Urukova, J. Vorholz, G. Maurer, J. Phys. Chem. B 109 (2005) 12154.
[34] C. Cadena, J.L. Anthony, J.K. Shah, T.I. Morrow, J.F. Brennecke, E.J. Maginn, J. Am. Chem. Soc. 126 (2004) 5300.
[35] X.C. Zhang, F. Huo, Z.P. Liu, W.C. Wang, W. Shi, E.J. Maginn, J. Phys. Chem. B 113 (2009) 7591.
[36] T. Seki, J.D. Grunwaldt, A. Baiker, J. Phys. Chem. B 113 (2009) 114.
[37] L. Cammarata, S.G. Kazarian, P.A. Salter, T. Welton, Phys. Chem. Chem. Phys. 3 (2001) 5192.
[38] M.G. Miles, G. Doyle, R.P. Cooney, R.S. Tobias, Spectrochim. Acta A A25 (1969) 1515.
[39] C.S. Chen, J.H. Lin, T.W. Lai, B.H. Li, J. Catal. 263 (2009) 155.
[40] E. Wieberg, Die chemische Affinität, second ed., de Gruyter, Berlin, New York, 1972.
[41] J.K. Shah, E.J. Maginn, J. Phys. Chem. B 109 (2005) 10395.
[42] D.R. Stull, H. Prophet, JANAF Thermochemical Tables, Nat. Bur. Stand. (US) (1971).